
INFLUENCE OF A SURFACE STATE AND SCREENING PHENOMENA ON THE NUCLEATION AND GROWTH OF ARTIFICIAL NANODOMAINS IN FERROELECTRICS-SEMICONDUCTORS¹

A.N. MOROZOVSKA, G.S. SVECHNIKOV, S.V. KALININ¹,
E.L. RUMYANTSEV², E.I. SHISHKIN², A.I. LOBOV², V.YA. SHUR²

UDC 532
©2008

V. Lashkarev Institute of Semiconductor Physics, Nat. Acad. Sci. of Ukraine
(45, Nauky Prosp., Kyiv 03028, Ukraine; e-mail: morozo@i.com.ua),

¹Condensed Matter Sciences Division, Oak Ridge National Laboratory
(Oak Ridge, TN 37831, USA),

²Institute of Physics and Applied Mathematics, Ural State University
(Ekaterinburg 620083, Russian Federation)

A review of recent theoretical studies of the effects of a surface state and the screening on the nucleation and growth of artificial nanodomains in ferroelectrics-semiconductors. The obtained results prove that the formation of nanodomains caused by the inhomogeneous electric field of a biased force microscope probe is a first-order phase transition, since the domains with finite radii appear at the critical voltage applied to the probe. The critical voltage depends on the probe geometry, films thickness, surface state, and screening effects. The activation barrier height and domain nucleus critical sizes strongly depend on the surface charge state: a value and the distribution of charge density that screen the spontaneous polarization outside the sample.

1. Introduction

Domains with almost homogeneous polarization and thin enough domain walls can be formed in ferroelectrics and ferroelectrics-semiconductors by a local external excitation caused by inhomogeneous electric fields with definite polarity.

Recently, one- and two-dimensional arrays of stable submicro- and nanodomains have been tailored in such ferroelectric materials as LiNbO₃, LiTaO₃, Pb(Zr,Ti)O₃, BaTiO₃, and BiFeO₃ with the help of the inhomogeneous electric field produced by the probe of an atomic force microscope (AFM)

or piezoelectric force microscope (PFM) [1–10]. The experimental and theoretical investigations of “artificial” domain structure tailoring are of high interest owing to their prospective applications in modern nanotechnology, design of nanoelectronic and electromechanic device elements, nonlinear optics, and memory cells.

From the fundamental point of view, the polarization reversal in nanoregions of polar-active materials by using AFM and PFM is a prospective field for *in situ* studies of the size and surface effects of the domain structure and the switching kinetics. The adequate model of local polarization switching is desirable for the further progress.

The totality of published experimental data corroborates the fact that defects and local mechanical stresses, size and surface effects, conductivity and thickness of samples, and properties of substrates and electrodes essentially affect the polarization reversal in nanoregions. However, the united notions about the defect influence on the mechanisms of domain nucleation, growth, and reversal are still absent. As a sequence, there are no explanation of the essential difference between calculated and measured coercive fields, quantitative description of a decrease of the

¹The results of the work were reported at the 3-rd Ukrainian Scientific Conference on Semiconductor Physics (17–22 June 2007, Odessa, Ukraine).

switchable charge under the switching cycling, and consideration of the realistic finite domain wall width.

While the macroscopic polarization switching has been studied in details, the kinetics of polarization reversal in nanodomain structures requires a complex experimental and theoretical investigation. In accordance with modern scientific conceptions, local methods of probe microscopy are ideal for the experimental study of the nanodomain formation; they not only accomplish optics methods but also have several specific advantages. Experimental and theoretical investigations of the polarization switching kinetics and the domain wall motion mechanism in typical ferroelectric materials like $\text{Pb}(\text{Zr}, \text{Ti})\text{O}_3$, $\text{Pb}_5\text{Ge}_3\text{O}_{11}$, LiTaO_3 , LiNbO_3 , and relaxor ceramics were reported in works [11–17]. The regimes of the fast and ultrafast motion of domain walls and the self-organization possibilities were demonstrated for the first time; the leading role of the depolarization field screening retardation was established. It was shown that the surface dielectric layer characteristics and the electrode type essentially influence the domain formation kinetics and a shape of separate domains.

A number of phenomenological models of domain formation in ferroelectric single crystals and thin films [18–22] is based on the classical thermodynamic approach formulated in [23], where the domain nucleation was studied in ferroelectrics-dielectrics under a *homogeneous* electric field. The model predicted extremely high activation barriers for the homogeneous domain nucleation, suggesting the role of defects in the polarization switching (the Landauer paradox). The surface bound charges on the domain face close to the electrode are compensated by the free charges on plain metallic electrodes, so that only the infinitely thin charged domain wall contributes to the depolarization field energy. In the majority of theoretical papers considering the artificial domain formation, semiconductor properties of ferroelectrics are neglected; the screening and the compensation of bound charges are not considered. These limitations make a lot of models self-contradictory. For instance, surface bound charges are regarded screened during the polarization reversal, while the interaction energy of a nucleated domain with an external electric field is calculated under the absence of screening charges. However, since the probe causes a strong inhomogeneous electric field near the ferroelectric surface, the recharging of surface levels is quite probable in the majority of experiments.

Within the modified Preisach approach, the difference between local coercive fields for the single-

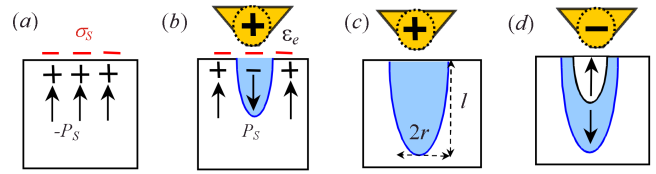


Fig. 1. Nanodomain formation stages caused by the electric field of a charged FM probe apex: (a) initial state, (b) nucleation, growth (c), reversal (d). U is electric voltage applied to the probe; ΔR is the distance between the probe apex and the sample surface, R_0 is the probe apex curvature, r is the semiellipsoidal domain radius, l is its length, h is the film thickness, P_S is the spontaneous polarization, and σ_S is the density of surface screening charges determined by the polarization bound charge abrupt at the surface

domain nucleation and a step on the domain wall appeared during the domain growth is taken into consideration. This allows one to model the domain kinetics in ferroelectrics with inhomogeneous spatial distributions of coercive fields and to distinguish the main stages of domain structure growth [24–26]. Special attention is paid to the retardation of depolarization field screening effects. Within the modified Preisach approach, it is possible to calculate the influence of a surface dielectric gap on the screening efficiency.

2. Problem

Following original papers [27–33], let us consider the thermodynamic formation of nanodomains caused by the biased probe inhomogeneous electric field allowing for semiconductor properties, surface and bulk screening charge layers, and size effects in thin ferroelectric films.

The sample is regarded as a transversely isotropic ferroelectric with spontaneous polarization vector \mathbf{P}_S and different values of dielectric permittivity along and across a polar axis, ε_{33} and ε_{11} , respectively. The polar axis z is directed across the surface inside the sample, so that the spontaneous polarization is $+P_S$ inside and $-P_S$ outside the domain (see Fig. 1). Within the rigid ferroelectric model, we suppose that the dependence of the susceptibility on an external field \mathbf{E} is small enough, so the displacement vector is $\mathbf{D} = \varepsilon_0 \varepsilon_{33} \mathbf{E} + \mathbf{P}_S$ (ε_0 is the universal dielectric constant).

For typical experiments performed in ambient (e.g., in air without special drying), the hydrophilic surface of oxide materials is covered with a thin water layer. When the charged microscope probe approaches the surface, polar water molecules are attracted by the strong electric field; in this case, the hydrophilic or hydrophobic probe

apex material and the water absorption and dissociation play an important role. Thus, we assume further that the ambient medium has dielectric permittivity ε_e , and $1 \leq \varepsilon_e \leq 81$.

Before the domain formation, surface bound charges with charge density P_S are fully compensated by ambient screening charges with charge density $\sigma_S^0 = -P_S$. The appearance of the screening charge layer can be related with a slow redistribution of surface free charges captured by deep surface layers, as well as the free charge segregation from ambient related to the absorption of water molecules.

Various models of screening charge layers appeared at a semiellipsoidal domain face (denoted as σ_S) and around the moving domain wall (denoted as σ_b) have been considered in [27–33]. Most acceptable is the model where a screening charge σ_b captured by the domain wall allowing for the band bending and the strong electric depolarization field is concentrated near the domain apex and thus screens the spontaneous polarization $+P_S$. The effect of the capture of screening charges by the moving domain wall is corroborated by numerous experimental facts proving that the neighboring domains in a dense array do not cross-talk during their formation, reorientation, and storage. Depending on the domain shape, σ_b and σ_S are different on the domain surface: $\sigma_b \rightarrow -(P_S + \sigma_S)$ near an oblate domain apex allowing for the initial screening charge conservation $\sigma_S^0 = -P_S$, while $\sigma_b \rightarrow -2P_S$ near the spike-like domain apex (see Fig. 1). In the general case, σ_S depends on the surface state and the electric field distribution near the surface (i.e. on the probe-sample surface geometry) and vary within the range $-P_S \leq \sigma_S \leq P_S$.

In the ferroelectric-semiconductor bulk, the charge density $\rho_f(\mathbf{r})$ satisfies the equation $\rho_f(\mathbf{r}) \approx -\varepsilon_0 \kappa \varphi(\mathbf{r})/R_d^2$ in the linear approximation, where R_d is the Debye screening radius and $\kappa = \sqrt{\varepsilon_{11}\varepsilon_{33}}$ is the effective dielectric constant. The potential distribution $\varphi(\mathbf{r})$ is determined by the Poisson equation with the boundary conditions for the potential and normal displacement components, $D_{n_{\text{ext}}} - D_{n_{\text{int}}} = \sigma_b(z)$ on the domain sidewall Σ , and $D_{n_{\text{ext}}} - D_{n_{\text{int}}} = \sigma_S$ on the sample surface $z = 0$.

The electric field induced by a biased probe, $\mathbf{E} = -\nabla\varphi(\mathbf{r})$ was calculated using the appropriate model for a probe tip. For the domain nucleation and initial growth stages, we use the local point charge model that adequately describes the probe electric field in the immediate vicinity of the tip-surface junction. For the later growth stages, one could use the more rigorous but complex sphere-plane model, when the conductive

probe apex is considered as a metallic sphere of radius R_0 under voltage U . The results obtained in the capacitance approximation (a point charge at distance R_0 from the surface) were analyzed for comparison.

3. Nanodomain Nucleation in Ferroelectrics-Semiconductors

The next step is to determine the electrostatic energy $\Delta\Phi_{\text{el}} = \Delta \int dv (\mathbf{D} \cdot \mathbf{E} - \mathbf{P}_S \cdot \mathbf{E})/2\varepsilon_0$ of the domain and the domain wall energy $\Phi_S(r, l)$, as described below.

When the electrostatic potential $\varphi(\mathbf{r})$ is determined, and the domain free energy is calculated, the nucleation conditions and the growth stages of equilibrium domains can be determined within the thermodynamic approach. The free energy excess of the semiellipsoidal domain with radius r and length l formed below the tip under the action of a bias U acquires the form [28–33]:

$$\Phi(U, r, l) = \Phi_U(U, r, l) + \Phi_S(r, l) + \Phi_D(r, l). \quad (1)$$

a) $\Phi_U(r, l)$ is the interaction energy of the domain polarization with the tip-induced inhomogeneous electric field; its Pade approximation has the form

$$\Phi_U(r, l) \approx \frac{R_d U C_t / \varepsilon_0}{(\kappa + \varepsilon_e) R_d + 2\kappa \sqrt{d^2 + r^2}} \times \left(\frac{(\sigma_S - P_S) r^2}{\sqrt{r^2 + d^2} + d} + \frac{(2P_S + \sigma_b) r^2}{\sqrt{r^2 + d^2} + d + (l/\gamma)} \right). \quad (2)$$

The distance d is the effective charge - surface separation describing the probe tip electric field (typically, $d = 1 - 100$ nm) and is proportional to the tip curvature R_0 and the tip apex-sample separation ΔR . The quantities ε_e and $\kappa = \sqrt{\varepsilon_{33}\varepsilon_{11}}$ are the ambient and ferroelectric dielectric permittivities, C_t is the probe tip effective capacity, and $\gamma = \sqrt{\varepsilon_{33}/\varepsilon_{11}}$ is the dielectric anisotropy factor. Under the typical conditions $R_0 \gg \Delta R$ and $R_d \gg R_0$, the distance $d = \varepsilon_e R_0 / \kappa$ and capacity $C_t \approx 2\pi\varepsilon_0 (\varepsilon_e + \kappa) d$ within the local point charge model. Within the total point charge model for a spherical tip apex of radius R_0 that touches the surface, $C_t \approx 4\pi\varepsilon_0 \varepsilon_e R_0 \frac{\kappa + \varepsilon_e}{\kappa - \varepsilon_e} \ln \left(\frac{\varepsilon_e + \kappa}{2\varepsilon_e} \right)$, $d \approx 2\varepsilon_e R_0 \ln((\varepsilon_e + \kappa)/2\varepsilon_e)/(\kappa - \varepsilon_e)$. In the capacitance approximation, $d = R_0 + \Delta R \approx R_0$, and C_t is the same as that for the total point charge model.

b) The domain wall surface energy $\Phi_S(r, l)$ is

$$\Phi_S(r, l) = \pi\psi_S l r \left(\frac{r}{l} + \frac{\arcsin \sqrt{1 - r^2/l^2}}{\sqrt{1 - r^2/l^2}} \right). \quad (3)$$

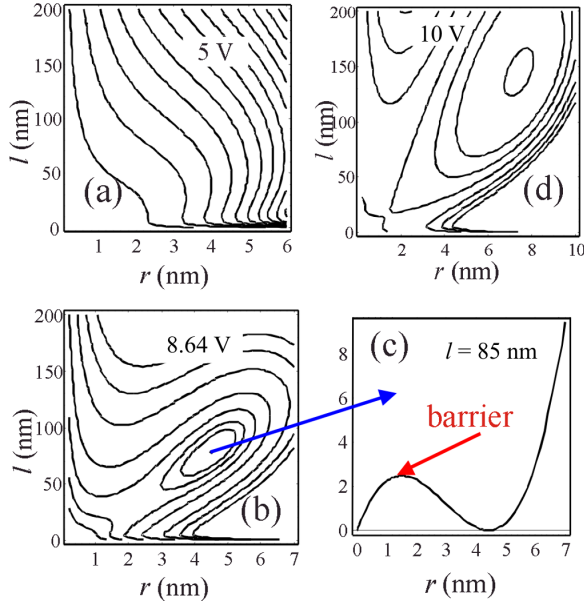


Fig. 2. Free energy contour maps $\Phi(r, l)$ of a semiellipsoidal domain for different voltages U applied to the probe: $U = 5; 8.5; 10$ V (a–d). Material parameters: $P_S \approx 0.6$ C/m², $\psi_S \approx 100$ mJ/m², $\epsilon_e = 10$, $\epsilon_{11} \approx \epsilon_{33} = 70$ corresponds to BiFeO₃; $\sigma_S = -P_S$, $\Delta R \leq 1$ nm, $R_0 = 50$ nm, $d = 7$ nm, $R_d > 500$ nm ($U_{cr} \approx 8.64$ V)

Here, we assume that the domain wall thickness is negligibly small in comparison with domain sizes, and the domain wall surface energy ψ_S is a constant independent of the wall orientation. In accordance with the recent data, the thickness of domain wall is of the order of several lattice constants in perovskite ferroelectrics. However, the value of ψ_S discrepancy encountered in the literature is very high, e.g., 1–10 mJ/m² for BaTiO₃ and 40–400 mJ/m² for LiTaO₃. Thus, ψ_S can be considered as a fitting parameter.

c) It has been shown [29–33] that the depolarization field energy is created by the bulk (Landauer contribution) and the surface charges. For the considered case of tip-induced nucleation, the Pade approximation of depolarization field energy $\Phi_D(r, l)$ is

$$\Phi_D(r, l) \approx \frac{4\pi r^3 R_d l (\sigma_S - P_S)^2}{\epsilon_0 (l (3\pi R_d (\kappa + \epsilon_e) + 16\kappa r) + 8\gamma \kappa R_d r)}. \quad (4)$$

The thermodynamics of the switching process can be analyzed from the bias dependence of the free energy, Eqs. (1)–(4). The dependence of $\Phi(r, l)$ on the domain radius r and the length l can be represented as a free energy surface for each value of U (see Fig. 2).

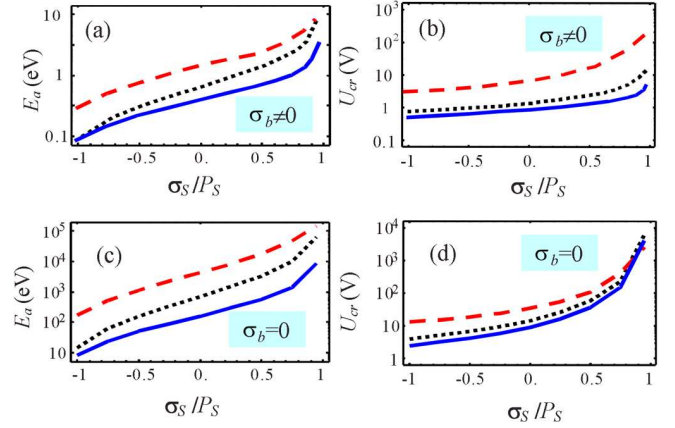


Fig. 3. Domain nucleus activation energy E_a at voltage $U = U_{cr}$ (a, c) and critical voltage U_{cr} (b, d) via the relative surface charge density σ_S (in spontaneous polarization P_S units) for $\sigma_b \neq 0$ (a, b) and $\sigma_b = 0$ (c, d). The solid curve is calculated for the effective point charge tip model, the dotted curve is calculated for the sphere-plane tip model, and the dashed curve represents the capacity approximation. Material parameters are the same as in Fig. 2

For small biases, $U < U_S$, the free energy is a positive definite monotonic function of domain sizes corresponding to the absence of a stable switched domain. At $U = U_S$, the saddle point appears. For biases $U_S < U < U_{cr}$, the local minimum $\Phi_{min} > 0$ corresponding to a metastable domain of size l, r arises. For $U = U_{cr}$, the absolute minimum $\Phi_{min} = 0$ corresponding to a thermodynamically stable domain of size l_{cr}, r_{cr} is achieved. The threshold corresponds to the first-order phase transition. For $U \geq U_{cr}$, the stable domain of sizes l, r is formed. The metastable or stable minimum point and the coordinate origin are separated by the saddle point $\{r_S, l_S\}$. The corresponding energy $\Phi(r_S, l_S) = E_a$ is the activation barrier for the domain nucleation, while the domain parameters $\{r_S, l_S\}$ represent the critical nucleus size.

The influence of surface screening on the activation barrier of the domain nucleus formation and the corresponding critical voltage is illustrated in Fig. 3 for the case $\sigma_b \neq 0$ (a, b) and $\sigma_b = 0$ (c, d). The activation barrier and the critical voltage are minimal for $\sigma_S = -P_S$ (less than 0.1 at $\sigma_b \rightarrow -2P_S$ and 10 eV at $\sigma_b = 0$). The barrier drastically increases (up to 10⁵ eV) at $\sigma_S \rightarrow +P_S$ and $\sigma_b = 0$. Such a behavior is related to the assumption about the absence of the carrier capture by the domain wall near the domain apex and the absence of a gap between the bound and screening charges on the domain face. Thus, the

screening charge increase (i.e. $\sigma_S > -P_S$) leads to a decrease of the electrostatic forces induced by a charged probe. In the case of complete screening ($\sigma_S \rightarrow P_S$), the electrostatic forces are absent, and the domain formation does not appear.

We note that the realistic barrier (less than 1 eV) calculated for prolate nuclei in the inhomogeneous electric field of a probe at $\sigma_S < 0.5P_S$ and $\sigma_b \rightarrow -2P_S$, is about 3–7 orders less than that in the case of a homogeneous electric field considered by Landauer. The barrier height rapidly decreases with increase in the voltage U . The activation energy and the critical voltage calculated within the capacitance model of probe (about 200 eV for $U_{cr} \approx 10$ V) are much more higher than the values calculated within the spherical and effective point charge models. Thermal domain nucleation is impossible for such high barriers, making the capacitance approximation widely used for the late growth stages to be inapplicable to calculations of the nucleation threshold. Analyzing the obtained results concerning the nucleation of a domain and its initial growth and calculated within different models of the electric field of a probe, we conclude that the effective point charge model is rather adequate and most simple.

The activation barrier height E_a , critical voltage U_{cr} , and nucleus sizes r_S and l_S depend on the screening charge density. In ferroelectrics-semiconductors, the screening mechanism of spontaneous polarization is essentially different for the $+Z$ and $-Z$ polar cuts. For instance, the carriers of different types (i.e. electrons and holes) have different mobilities and electrochemical potentials which determine the work function [since different ions (Li–O or Nb–O) are located at the $+Z$ and $-Z$ cuts, respectively]. This leads to the different values of U_{cr} for the $+Z$ and $-Z$ cuts. That is why the experimentally obtained critical voltage and minimal domain sizes at different polar cuts of LiNbO₃ and LiTaO₃ differ by several times under the other conditions being the same [34].

Additional calculations have shown that the Debye screening leads to the approximately identical decrease in both the electric field of a probe inside the sample and the depolarization field. The growth of the domain radius almost stops at $r \gtrsim R_d$, and the increase in the length stops at $l \gtrsim R_d$. To the best of our knowledge, stable domains of submicron and micron sizes can be formed in stoichiometric LiNbO₃ and LiTaO₃ single crystals in dry atmosphere (argon) after a special surface treatment. The domain radius is not more than 100–200 nm in ferroelectrics-semiconductors such as doped

Pb(Zr,Ti)O₃, BaTiO₃, or BiFeO₃ in agreement with estimations $R_d = 50 \div 500$ nm.

At $R_d \gg l$, the approximate analytical expressions for the critical voltage U_{cr} and sizes r_{cr} , l_{cr} , equilibrium domain sizes $\{r_{eq}, l_{eq}\}$ in terms of the applied voltage U are given in [32, 33]. The expression for the effective piezoelectric response d_{33}^{eff} measured at the center of a rather prolate ($r \ll l$) or cylindrical domain with radius r_{eq} was derived in [35]. The piezoelectric response of thin films was analyzed in [36, 37]. Expressions which provide the self-consistent analysis of the effective piezoelectric response d_{33}^{eff} as a function of the applied voltage U have the form

$$d_{33}^{eff}(r_{eq}) \approx - \left(\frac{3d_{33}^*}{4} \left(1 - \frac{2}{1 + \pi d/8r_{eq}} \right) + \frac{d_{15}}{4} \left(1 - \frac{2}{1 + 3\pi d/8r_{eq}} \right) \right), \quad (5a)$$

$$r_{eq}(U) \approx r_{cr} \left(1 + 2 \sqrt{\frac{2d}{3r_{cr}} \left(\frac{U}{U_{cr}} - 1 \right)} \right),$$

$$l_{eq}(U) \approx l_{cr} \left(1 + 2 \sqrt{\frac{2d}{r_{cr}} \left(\frac{U}{U_{cr}} - 1 \right)} \right). \quad (5b)$$

Here, $d_{33}^* = d_{33} + (1/3 + 4\nu/3)d_{31}$, d_{ij} is the strain piezoelectric tensor, $\nu \approx 0.35$ is the Poisson's ratio, and the dielectric anisotropy is small, i.e. $\gamma \approx 1$.

It is worth noting that the experimentally observed saturation law for PFM response hysteresis loops corresponding to the domain formation and the reversal differs from expressions (5) obtained in the absence of the domain wall pinning for constant piezoelectric coefficients d_{ij} . To describe the realistic piezoelectric response loops, both the pinning phenomena and the voltage dependence of d_{ij} should be taken into account, because, by definition, $d_{ij} \sim \varepsilon_{kj}(U)P_S(U)$, where the dielectric permittivity $\varepsilon_{kj}(U)$ and the polarization $P_S(U)$ depend on the applied voltage U in agreement with the dielectric and ferroelectric hystereses.

4. Thermodynamics of Nanodomain Formation in Thin Films of Ferroelectrics-Semiconductors

For the miniaturization of devices, the nanodomain formation in ferroelectric films of thickness less than 100–200 nm is much more expedient, than the usage of samples with micron thickness. As was shown in [22, 28],

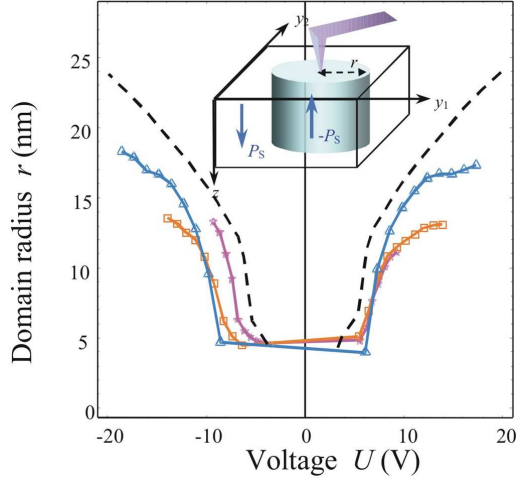


Fig. 4. Domain radius r versus the applied voltage U for a BiFeO₃ film with the thickness $h = 240$ nm obtained by the deconvolution of a piezoresponse hysteresis loop at maximal voltages $U = 10, 15$ and 20 V (points). The thermodynamic dependence of the domain radius on the applied voltage is shown by the dashed curve. Experimental data are taken from [38]. For the deconvolution, Eq. (12) was used at $d_{33}^* = d_{15} = 54$ pm/V and $d = 7$ nm. The calculated effective point charge-surface separation $d = 7$ nm corresponds to the tip apex curvature $R_0 = 50$ nm and the ambient medium susceptibility $\varepsilon_e = 10$. The parameters for the thermodynamic dependence $r(U)$ corresponding to the activation barrier $E_a < 1$ eV are listed in the capture of Fig. 5. The inset shows the geometry taken in the piezoelectric response calculations at the center of a cylindrical domain

the domain formation caused by the inhomogeneous electric field of a charged probe demonstrates four successive stages with increase in the applied voltage: (a) the nucleation of a new domain under the action of voltages more than U_{cr} , which depends on the tip geometry, film thickness, screening, and a state of the surface; (b) the growth of a semiellipsoidal domain; (c) the instability region when the domain wall approaches the bottom electrode; and (d) a cylindrical domain runs through the film from the free surface to the bottom electrode and the further growth occurs in the lateral direction only.

Analytical and numerical calculations have shown that domains usually transpierce films of thickness $h \ll \kappa R_0$.

For the stage of lateral domain growth, the free energy of a cylindrical domain transpierced the film has the form similar to Eq. (1), i.e. $\Phi(r) = \Phi_S(r) + \Phi_U(r) + \Phi_D(r)$. Under the condition $\Delta R \ll R_0$ typical of the majority of experiments on the domain formation, the following expressions are valid [28]:

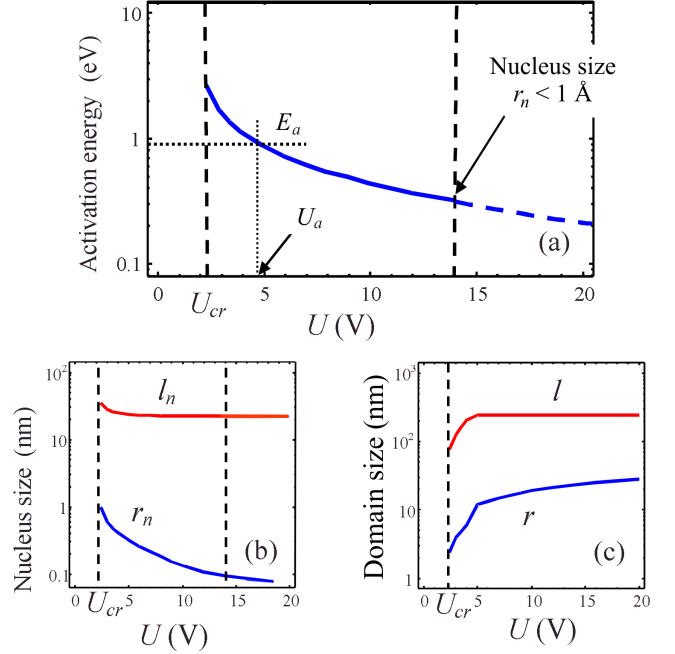


Fig. 5. Activation energy (a), critical nucleus sizes (b) and equilibrium domain sizes (c) versus the applied voltage U for a 240-nm-thick BiFeO₃ film calculated within the effective point charge model of the electric field of a probe tip. The jump on the dependence $r(U)$ indicates the penetration of the domain through the film. The parameters are listed in Fig. 2; $\sigma_S = -0.25P_S$

a) Domain wall energy:

$$\Phi_S(r) = 2\pi\psi_S r h; \quad (6)$$

b) Pade approximation for the energy of interaction of the domain polarization with the tip-induced inhomogeneous electric field calculated within the sphere-plane model of the electric field of a probe tip:

$$\Phi_U(r) = \frac{\kappa + \varepsilon_e}{\kappa - \varepsilon_e} \ln \left(\frac{\kappa + \varepsilon_e}{2\varepsilon_e} \right) \times \frac{4\pi\varepsilon_e (\sigma_S - P_S) R_0 h R_d \left(\sqrt{R_0^2 + r^2} - R_0 \right)}{(\kappa + \varepsilon_e) h R_d + \kappa(R_d + 2h) \sqrt{R_0^2 + r^2}} U; \quad (7)$$

c) the energy of the depolarization field created by surface bound charges:

$$\Phi_{DS}(r) \approx \frac{1}{\varepsilon_0} \frac{4\pi (\sigma_S - P_S)^2 r^3 h R_d}{(16\kappa r + 3\pi (\kappa + \varepsilon_e) R_d) h + 8\kappa R_d r}. \quad (8)$$

If the difference $(P_S - \sigma_S)$ is positive and does not tend to zero, the equilibrium domain radius r overcomes

the probe apex radius R_0 and can be described by the following voltage dependence:

$$r \approx \frac{R_d h (\kappa + \varepsilon_e)}{(R_d + 2h) \kappa} \left(\left[\frac{2(P_S - \sigma_S) \varepsilon_e}{\psi_S h (\kappa - \varepsilon_e)} \ln \left(\frac{\kappa + \varepsilon_e}{2\varepsilon_e} \right) \times \right. \right. \\ \left. \left. \times R_0 \left(\frac{R_0 (R_d + 2h) \kappa}{R_d h (\kappa + \varepsilon_e)} + 1 \right) \right]^{1/2} - 1 \right). \quad (9)$$

Domain radius can be determined from experimentally obtained piezoresponse hysteresis loops by the deconvolution method using Eqs. (5a), (5b), and/or (9). The typical dependence of the domain radius on the applied voltage and the calculated thermodynamic curve are shown in Fig. 4 for a multiferroic BiFeO₃ film.

Analyzing the difference between the thermodynamic dependence (the dashed curve) and the deconvolution (points), it is possible to estimate the quantitative influence of defects on domain sizes. At small voltages ($U < 10$ V), the thermodynamic curve and the deconvolution are relatively close to each other, i.e. the defects which are far from the nucleation region weakly affect the local polarization switching kinetics in BiFeO₃. As the voltage increases ($U > 10$ V), the domain radius increases, the electric field on its boundary decreases, and the domain wall pinning becomes noticeable: the thermodynamic curve corresponds to higher domain radii than the realistic “admixture” of kinetics and thermodynamics.

5. Conclusions

The nucleation of nanodomains in ferroelectrics-semiconductors is the first-order phase transition. A nucleus overcomes the activation barrier, and a domain appears with finite radius at the definite critical voltage applied to the probe.

The leading role of surface screening during the domain nucleation, equilibrium growth, and reversal induced by the electric field of a probe in ferroelectrics-semiconductors is established. Additionally, both the surface and bulk screenings lead to the saturation of the domain radius and length at the later growth stages.

For the rigorous description of the local polarization switching on the real time scale, the domain wall pinning should be considered. The thermodynamical approach allows the description of piezoresponse hysteresis loops which correspond to the nanodomain nucleation, growth, and polarization reversal.

The obtained results allow one to clarify the physical processes running during the nanoscale polarization reversal in ferroelectrics-semiconductors and open a way of the optimization of experimental conditions for the formation of stable ferroelectric nanostructures by scanning probe microscopy.

1. J. Woo, S. Hong, N. Setter, H. Shin, J.-U. Jeon, Y.E. Pak, and K. No, *J. Vac. Sci. Technol. B* **19**, 818 (2001).
2. B.J. Rodriguez, R.J. Nemanich, A. Kingon, A. Gruverman, S.V. Kalinin, K. Terabe, X.Y. Liu, and K. Kitamura, *Appl. Phys. Lett.* **86**, 012906 (2005).
3. M.I. Molotskii and M.M. Shvebelman, *Phil. Mag.* **85**, 1637 (2005).
4. M. Abplanalp, *Piezoresponse Scanning Force Microscopy of Ferroelectric Domains*, Ph.D. thesis (Swiss Federal Institute of Technology, Zurich, 2001).
5. A. Agronin, M. Molotskii, Y. Rosenwaks, G. Rosenman, and B.J. Rodriguez, *J. Appl. Phys.* **99**, 104102 (2006).
6. Y. Cho, S. Hashimoto, N. Odagawa, K. Tanaka, and Y. Hirayama, *Nanotechnology* **17**, S137 (2006).
7. X. Zhanga, D. Xuea, X. Liub, and K. Kitamura, *Physica B* **387**, 147 (2007).
8. X. Zhang, *J. Phys. D: Appl. Phys.* **39**, 3103 (2006).
9. P. Paruch, T. Tybell, and J.-M. Triscone, *Appl. Phys. Lett.* **79**, 530 (2001).
10. K. Fujimoto and Y. Cho, *Appl. Phys. Lett.* **83**, 5265 (2003).
11. V.Ya. Shur, E.L. Rumyantsev, E.V. Nikolaeva, E.I. Shishkin, D.V. Fursov, R.G. Batchko, L.A. Eyres, M.M. Fejer, and R.L. Byer, *Appl. Phys. Lett.* **76**, 143 (2000).
12. V.Ya. Shur, E.V. Nikolaeva, and E.I. Shishkin, *Phys. Low-Dimen. Struct.* **3/4**, 139 (2003).
13. V.Ya. Shur, G.G. Lomakin, E.L. Rumyantsev, O.V. Yakutova, D.V. Pelegov, A. Sternberg, and M. Kosec, *Fiz. Tverd. Tela* **47**, 1293 (2005).
14. E.I. Shishkin, V.Ya. Shur, F. Schlaphof, and L.M. Eng, *Appl. Phys. Lett.* **88**, 252902 (2006).
15. V.Ya. Shur, E.L. Rumyantsev, E.V. Nikolaeva, and E.I. Shishkin, *Integrated Ferroelectrics* **59**, 1493 (2003).
16. V.Ya. Shur, I.S. Baturin, and E.L. Rumyantsev, *Ferroelectrics* **349**, 163 (2007).
17. V.Ya. Shur, E.L. Rumyantsev, A.G. Shur, A.I. Lobov, D.K. Kuznetsov, E.I. Shishkin, E.V. Nikolaeva, M.A. Dolbilov, P.S. Zelenovskiy, K. Gallo, and M.P. De Micheli, *Ferroelectrics* **354**, 145 (2007).
18. M. Molotskii, *J. Appl. Phys.* **93**, 6234 (2003).
19. M. Molotskii, A. Agronin, P. Urenski, M. Shvebelman, G. Rosenman, and Y. Rosenwaks, *Phys. Rev. Lett.* **90**, 107601 (2003).
20. M. Shvebelman, *Static and Dynamic Properties of Ferroelectric Domains Studied by Atomic Force Microscopy*. Ph.D. Thesis (Tel Aviv University, Tel Aviv, 2005).
21. S.V. Kalinin, A. Gruverman, B.J. Rodriguez, J. Shin, A.P. Baddorf, E. Karapetian, and M. Kachanov, *J. Appl. Phys.* **97**, 074305 (2005).

22. A.Yu. Emelyanov, Phys. Rev. B **71**, 132102 (2005).
23. R. Landauer, J. Appl. Phys. **28**, 227 (1957).
24. V.Ya. Shur, E.L. Rumyantsev, E.V. Nikolaeva, E.I. Shishkin, and I.S. Baturin, J. Appl. Phys. **90**, 6312 (2001).
25. V.Ya. Shur, J. Mater. Sci. **41**, 199 (2006).
26. E.I. Shishkin, V.Ya. Shur, O. Mieth, L.M. Eng, L.L. Galambos, and R.O. Miles, Ferroelectrics **340**, 129 (2006).
27. A.N. Morozovska, Semicond. Phys. Quant. Electr. Optoelectr. **9**, 26 (2006).
28. A.N. Morozovska, and E.A. Eliseev, Phys. Rev. B **73**, 104440 (2006).
29. A.N. Morozovska, E.A. Eliseev, S.V. Kalinin, App. Phys. Lett. **89**, 192901 (2006).
30. A.N. Morozovska, S.V. Svechnikov, E.A. Eliseev, S. Jesse, B.J. Rodriguez, and S.V. Kalinin, J. Appl. Phys. **102**, 114108 (2007).
31. A.N. Morozovska, S.V. Kalinin, E.A. Eliseev, and S.V. Svechnikov, Ferroelectrics **354**, 198 (2007).
32. A.N. Morozovska, S.V. Kalinin, E.A. Eliseev, and S.V. Svechnikov, E-print cond-mat/0702221 (2007).
33. A.N. Morozovska, S.V. Svechnikov, E.A. Eliseev, S. Jesse, B.J. Rodriguez, S.V. Kalinin, E-print <http://arxiv.org/abs/0711.1426> (2007).
34. D. Xue, S. Wu, Y. Zhu, K. Terabe, K. Kitamura, and J. Wang, Chem. Phys. Lett. **377**, 475 (2003).
35. A.N. Morozovska, S.L. Bravina, E.A. Eliseev, and S.V. Kalinin, Phys. Rev. B **75**, 174109 (2007).
36. A.N. Morozovska, S.V. Svechnikov, E.A. Eliseev, and S.V. Kalinin, Phys. Rev. B **76**, 054123 (2007).
37. A.N. Morozovska, E.A. Eliseev, and S.V. Kalinin, J. Appl. Phys. **102**, 074105 (2007).
38. S.V. Kalinin, B. J. Rodriguez, S. Jesse, Y.H. Chu, T. Zhao, R. Ramesh, S. Choudhury, L.-Q. Chen, E.A. Eliseev, and A.N. Morozovska, Proc. Nat. Acad. Sci. of USA **104**, 20204 (2007).

Received 13.11.07

ВПЛИВ СТАНУ ПОВЕРХНІ І ЯВИЩ ЕКРАНУВАННЯ
НА НУКЛЕАЦІЮ І РІСТ ШТУЧНИХ НАНОДОМЕНІВ
У СЕГНЕТОЕЛЕКТРИКАХ-НАПІВПРОВІДНИКАХ

*Г.М. Морозовська, Г.С. Свечніков, С.В. Калінін,
Є.Л. Румянцев, Є.І. Шишкін, А.І. Лобов, В.Я. Шур*

Резюме

Представлено авторський огляд останніх теоретичних досліджень впливу стану поверхні та явищ екранування на нуклеацію та ріст штучних нанодоменів У сегнетоелектриках-напівпровідниках. Одержані результати вказують на те, що виникнення доменів під дією неоднорідного електричного поля зонда силового мікроскопа є фазовим переходом першого роду – домени скінченного радіуса утворюються, якщо електрична напруга, прикладена до зонда, вища за критичне значення, яке залежить від геометрії голки, товщини плівки, явищ екранування та стану поверхні. Висота енергетичного бар'єра і критичні розміри зародка в значній мірі визначаються станом поверхні зразку: величиною і розподілом густини заряду, що екранує спонтанну поляризацію зовні зразка.